Catalysis Today 144 (2009) 292–305

Contents lists available at ScienceDirect

Catalysis Today

journal homepage: www.elsevier.com/locate/cattod

Nanodispersed Au/Al_2O_3 catalysts for low-temperature CO oxidation: Results of research activity at the Boreskov Institute of Catalysis

B.L. Moroz [a,b,*], P.A. Pyrjaev [a], V.I. Zaikovskii [a,b], V.I. Bukhtiyarov [a,b]

[a] G.K. Boreskov Institute of Catalysis, Siberian Branch of Russian Academy of Sciences, 5 Avenue Akademika Lavrentieva, 630090 Novosibirsk, Russia
[b] Novosibirsk State University, 630090 Novosibirsk, Russia

ARTICLE INFO

Article history:
Available online 21 December 2008

Keywords:
Low-temperature CO oxidation
Au/Al_2O_3 catalysts
Gold dispersion

ABSTRACT

This paper presents some important results of the studies on preparation and catalytic properties of nanodispersed Au/Al_2O_3 catalysts for low-temperature CO oxidation, which are carried out at the Boreskov Institute of Catalysis (BIC) starting from 2001. The catalysts with a gold loading of 1–2 wt.% were prepared *via* deposition of Au complexes onto different aluminas by means of various techniques ("deposition-precipitation" (DP), incipient wetness, "chemical liquid-phase grafting" (CLPG), chemical vapor deposition (CVD)). These catalysts have been characterized comparatively by a number of physical methods (XRD, TEM, diffuse reflectance UV/vis and XPS) and catalytically tested for combustion of CO impurity (1%) in wet air stream at near-ambient temperature. Using the hydroxide or chloride gold complexes capable of chemical interaction with the surface groups of alumina as the catalyst precursors (DP and incipient wetness techniques, respectively) produces the catalysts that contain metallic Au particles mainly of 2–4 nm in diameter, uniformly distributed between the external and internal surfaces of the support granules together with the surface "ionic" Au oxide species. Application of organogold precursors gives the supported Au catalysts of egg shell type which are either close by mean Au particle size to what we obtain by DP and incipient wetness techniques (CVD of $(CH_3)_2Au(acac)$ vapor on highly dehydrated Al_2O_3 in a rotating reactor under static conditions) or contain Au crystallites of no less than 7 nm in size (CLPG method). Regardless of deposition technique, only the Cl-free Au/Al_2O_3 catalysts containing the small Au particles ($d_i \leq 5$ nm) reveal the high catalytic activity toward CO oxidation under near-ambient conditions, the catalyst stability being provided by adding the water vapor into the reaction feed. The results of testing of the nanodispersed Au/Al_2O_3 catalysts under conditions which simulate in part removal of CO from ambient air or diesel exhaust are discussed in comparison with the data obtained for the commercial Pd and Pt catalysts under the same conditions.

1. Introduction

For a long time, metallic gold was considered as a bad catalyst. However, as was discovered in 1987 by Haruta et al. [1], Au particles with a size of <5 nm supported on some metal oxides manifested a very high catalytic activity in oxidation of carbon monoxide at ambient temperature. In succeeding years, the number of communications devoted to catalytic properties of nanosized Au particles has progressively increased, especially very rapidly from 1997 [2]. It was shown that they are also catalytically active in a series of practically important reactions including hydrocarbon selective oxidation [3] and hydrogenation [4], water–gas shift reaction [5], *etc.* At the same time, low-temperature CO oxidation is still considered most promising area for application of supported Au catalysts. The possibilities of using gold catalysts for indoor air-quality and industrial pollution control, automobile exhaust gas treatment (in particular, during the period of engine "cold start"), removal of CO from hydrogen fuel for fuel cells, for applications in gas masks, as CO sensors, *etc.* are extensively studied [6].

It is commonly known that the catalytic activity of gold nanoparticles in CO oxidation is strongly dependent on the support nature [7–9]. Most active catalysts were prepared by depositing gold onto first-raw transition metal oxides (TiO_2, Co_3O_4, Fe_2O_3, NiO) as well as onto $Be(OH)_2$ and $Mg(OH)_2$. These catalysts were studied in sufficient detail but, for different reasons, they are not suitable for large-scale applications.

From the practical point of view alumina would be preferable support for Au catalysts as compared with other metal oxides

* Corresponding author at: G.K. Boreskov Institute of Catalysis, Siberian Branch of Russian Academy of Sciences, 5 Avenue Akademika Lavrentieva, 630090 Novosibirsk, Russia. Tel.: +7 3833269521; fax: +7 3833308056.
E-mail address: blmoroz@mail.ru (B.L. Moroz).

0920-5861/$ – see front matter © 2008 Elsevier B.V. All rights reserved.
doi:10.1016/j.cattod.2008.10.038

because of its cheapness, high and thermally stable surface area, well controllable porosity, and relative inertness toward steam. That is why we chose the "gold on alumina" catalysts prepared by different techniques as the principal objects for our own research on catalysis by gold which has started since 2001 in the Laboratory of Surface Studies at the Boreskov Institute of Catalysis (BIC). The main aims of our studies are as follows: (1) characterization of activity and stability of Au/Al_2O_3 catalysts in low-temperature CO oxidation depending on the catalyst preparation procedure and reaction conditions; (2) elucidation and investigation of reasons (including size effect) determining the catalytic activity of Au nanoparticles in CO oxidation; (3) optimization of methods for preparation of nanosized Au particles supported on various modifications of Al_2O_3; (4) estimation of potentialities of Au/Al_2O_3 catalysts as applied for combustion of CO impurities contained in air and automobile exhaust. Some important results obtained are discussed in the paper.

2. Experimental

2.1. Catalyst preparation

Microspherical γ-Al_2O_{3ms} (BIC; particle size, 0.5–0.7 mm; BET surface area, 185 m^2/g) pre-calcined in a dry airflow at 700 °C, an ultrathermostable θ-Al_2O_3 powder (Sasolchemie GmbH, Germany; particle size, 0.2–0.5 mm; BET surface area, 110 m^2/g) pre-calcined in a dry airflow at 600 °C, and commercial "active alumina" of AOA-2 grade (Dneprodzerzhinsk, Ukraine; particle size, 1–3 mm) were used as supports. A sample of AOA-2 representing initially a mixture of γ–χ-Al_2O_3 and pseudoboehmite AlOOH (30–40 wt.% AlOOH) was calcined in air at 475 °C for 6 h to convert it to almost pure γ-Al_2O_3 (lattice constant a = 0.798 nm) with the BET surface area of 250 m^2/g.

The nanodispersed Au/Al_2O_3 catalysts were prepared by the following techniques: (1) adsorption of anionic gold hydroxyl complexes from an alkalized aqueous solution of $HAuCl_4$ (the so-called "deposition-precipitation" method [10]); (2) incipient wetness impregnation using an aqueous $HAuCl_4$ solution; (3) adsorption of organogold complex from a non-polar organic solvent (the "chemical liquid-phase grafting" method [11]); (4) chemical vapor deposition of a highly volatile organogold precursor on a support surface at subatmospheric pressure.

2.1.1. "Deposition-precipitation" (DP)

A support was treated with an aqueous $HAuCl_4$ + NaOH solution at certain pH and temperature for 1 h, washed several times with large portions of warm distilled water (200 mL H_2O/1 g sample), dried and calcined in air at 400 °C for 4 h.

2.1.2. Incipient wetness impregnation (IMP)

A solution of $HAuCl_4$ taken at a required concentration was added to a weighed amount of Al_2O_3, the volume of the impregnating solution being equal to the total pore volume of the support. The resulting paste was mixed for 1 h and allowed to stay at 20 °C for 20 h. The impregnated '$HAuCl_4$'/Al_2O_3 samples were dried in air at 110 °C overnight and reduced with H_2 at 400 °C for 4 h.

2.1.3. "Chemical liquid-phase grafting" (CLPG)

A weighed amount of γ-Al_2O_{3ms} previously dehydrated at 300 °C under air was immersed in a fresh pentane solution of $(CH_3)_2AuL$ (L = acetyl acetonate (acac) or dipivaloyl methanoate (dpm)) synthesized by a procedure described elsewhere [12]. The suspension was vigorously stirred at 20 °C for 4 h and allowed to stay at 7–10 °C overnight. The sample was suction filtered, outgassed at 20 °C and calcined in air at 400 °C for 4 h in a muffle furnace pre-heated to this temperature.

2.1.4. Chemical vapor deposition (CVD)

Among several tested dimethylgold(III) chelates, for further CVD experiments we chose dimethylgold(III) acetylacetonate as the precursor for preparation of supported Au catalysts due to its accessibility, high volatility and thermal stability (saturated vapor pressure is 5.5×10^{-2} Pa at 25 °C; decomposition temperature in vapor state is 54 °C) [13]. To prepare the supported Au catalysts by the CVD technique we employed two different approaches. The first approach was to pass $(CH_3)_2Au(acac)$ vapor through a stainless steel column containing a fixed bed of γ-Al_2O_{3ms} which was preliminarily evacuated at 100 °C to 10^{-5} Pa and cooled to room temperature. Then air was admitted into the column, and the sample was calcined at 325 °C for 0.5 h. In the second approach, γ-Al_2O_{3ms} (0.5 g) was loaded in a glass ampoule (reactor) connected to a MI-1201 mass-spectrometer through a vacuum leak valve for on-line monitoring of the composition of the gas phase (sampling rate 0.1 cm^3/s). The support was evacuated at 300–350 °C and 10^{-5} Pa until the water peak vanished from the mass spectrum of the gas phase. After the reactor was cooled to room temperature, it was filled with $(CH_3)_2Au(acac)$ vapor and vertically rotated at a constant rate. As soon as the signals derived from the complex were not detected by mass spectrometry any more, another portion of the complex was introduced in the reactor, and this was repeated until the support surface was saturated with the adsorbed complex or until the whole amount of the complex (6 mg) evaporated. Then air was admitted into the reactor, the sample was heated in air up to 325 °C and calcined at this temperature for 0.5 h. The more detailed information about the experimental procedures and apparatus for preparation of Au/Al_2O_3 catalysts by CVD is presented in our article [13].

2.2. Catalyst characterization

The Au and Cl contents of the catalysts were measured using X-ray fluorescence (XRF) technique on a VRA-30 instrument equipped with a Cr-anode. The diffuse reflectance UV–vis spectra were recorded on a Shimadzu UV-2501 PC spectrometer equipped with an ISR-240 integrating sphere attachment for diffuse reflectance measurements, using $BaSO_4$ as a reference, in the range of 10,000–50,000 cm^{-1} and presented in Kubelka–Munk function $F(R)$—wavenumber coordinates. The transmission UV–vis spectra of solutions of colloidal gold and gold complexes were obtained using a quartz cell with a path length of 2 mm, with water as a reference liquid. X-ray diffraction (XRD) was performed using a HZG-4 X-ray diffractometer with Cu Kα radiation and a graphite monochromator. The data were collected for 5 s per step with a step size of 0.05° within the range of $20° \leq 2\theta \leq 90°$. Transmission electron microscopy (TEM) studies were carried out on a JEOL JEM-2010 electron microscope operated at 200 kV and giving an information limit of 0.14 nm. Prior to TEM study, a sample was ground and suspended in ethanol. A drop of suspension was mounted on a copper grid coated with a holey carbon film, and the solvent was allowed to evaporate. X-ray photoelectron (XP) spectra were measured with a VG ESCALAB HP photoelectron spectrometer using a non-monochromatized Al Kα radiation ($E_{h\nu}$ = 1486.6 eV) operated at 200 W as the excitation source. The binding energy (E_b) scale was calibrated against the positions of the Au $4f_{7/2}$ (E_b = 84.0 eV) and Cu $2p_{3/2}$ (E_b = 932.6 eV) core level peaks from polycrystalline foils of gold and copper, respectively. The samples were loaded in the form of granules or powder applied to conductive double-sided scotch. The charging effect was corrected using the Al 2p peak from Al_2O_3 at 74.5 eV as the

internal reference. The charging value was determined as the difference between the measured and tabulated E_b values of the Al 2p core level. The atomic surface content Au/Al and Cl/Au ratios were determined from the integrated intensities of the Au $4f_{7/2}$, Al 2p and Cl 2p core level peaks using atomic sensitivity factors [14].

2.3. Catalyst testing

For characterizing the performance of the Au/Al_2O_3 catalysts in CO oxidation with excess O_2, continuous flow experiments were performed at atmospheric pressure and constant temperature (40 °C) in a U-shaped glass reactor of 4 mm i.d. A catalyst sample (50–150 mg) diluted with quartz beads was placed between two pieces of glass fiber. The reaction mixture containing CO (1.0%), H_2O (2.4%), O_2 (20%), and N_2 (balance) was fed to the reactor through electronic mass-flow controllers at gas-hourly space velocity (GHSV) from 60,000 to 240,000 h^{-1}. Immediately before testing, the catalyst was treated at 150 °C for 1 h in an airflow containing 2.4% H_2O (GHSV = 60,000 h^{-1}). The CO and CO_2 contents in the inlet and outlet gas streams were on-line determined with a PEM-2M infrared gas analyzer (the relative measurement error was inferior to 5%). The catalytic performance was evaluated by CO conversion (χ) determined at certain catalyst amount, feed flow, and run time, and by the reaction rate (W) expressed per gram of gold and calculated from the outlet concentrations of CO or CO_2, which were measured under differential conditions (at $\chi \leq 25\%$) after the catalyst reached its steady state. Upon measuring the temperature dependence of the reaction rate, the reactor temperature was raised stepwise from 40 to 90 °C at a step of Δ = 10 °C; the reaction rate was calculated from the steady-state outlet CO and CO_2 concentrations measured at a given temperature under differential conditions. During all tests, the carbon balance between the feed and outlet stream was within 100 ± 3%.

The performance of the Au and Pd catalysts for oxidation of CO impurity contained in a wet airflow was compared using a test unit which allowed several catalyst samples to be tested simultaneously in parallel flow glass reactors of 20 mm i.d. at ambient temperature and pressure. The airflow at 85% relative humidity containing 450 ppm CO was passed through the bed of each catalyst (h = 3 cm) at GHSV = 20,000 h^{-1} for 7 h. The outlet gas mixture was analyzed using a gas chromatograph equipped with a flame ionization detector (FID). Carbon monoxide was quantitatively hydrogenated over a Ni catalyst to methane for further detection by FID (the detection limit for CO is 1 ppm).

Temperature-programmed reaction experiments were performed in a plug-flow U-shaped quartz reactor equipped with a coaxial thermocouple for temperature monitoring. The granular catalyst (0.7–1.0 cm^3) was loaded after being mixed with an equal volume of quartz beads. The reaction mixture containing CO (0.1%), H_2O (10%), O_2 (14%), and N_2 (balance) was introduced in the reactor at GHSV = 18,300–200,000 h^{-1}, and the temperature was raised with a constant heating rate of 10 °C/min from 30 to 300 °C. Then the system was maintained isothermally at 300 °C for 30 min under the reactant mixture stream, cooled down to 30 °C in flowing air, and the test was repeated. In order to examine the thermal and moisture stability of the catalysts, they were subjected to thermal-steam aging at 700 °C in flowing air containing 10% H_2O (GHSV = 18,300 h^{-1}) for 4 h. The aged catalysts were tested under the conditions identical to testing of the fresh catalyst. The inlet and outlet concentrations of CO, O_2, N_2 and H_2O were monitored on-line by a gas chromatograph. The results obtained were plotted as temperature dependencies of CO conversion (light-off curves). The temperature at which 50% of CO conversion is reached (light-off temperature or T_{50}) was determined from the light-off curves and used as a measure of the catalyst activity.

3. Results and discussion

3.1. Chemical species and dispersion of gold in the Au/Al_2O_3 catalysts

Table 1 shows the main characteristics of the Au/Al_2O_3 catalysts under discussion such as grades of alumina used, Au and Cl contents, the fraction of intended gold deposited on the support, and average Au particle sizes determined by TEM and XRD.

3.1.1. Catalysts prepared by DP

The treatment of aluminas with the $HAuCl_4$ + NaOH solution followed by washing and drying produced uncolored or light lilaceous samples which turned to dark violet upon calcination in air at 400 °C. Regardless of alumina modification, the catalysts prepared contain only a share of intended gold loading (Table 1). According to ICP-AES data, the amount of gold remaining in the $HAuCl_4$ + NaOH solution after its interaction with Al_2O_3 does not exceed 3–4% of its initial quantity. At the same time, the Au content in the resulting catalyst continuously decreases with an increase in the number of washing steps (Fig. 1). These data lead to conclude that the gold complexes are extracted fully enough from the liquid phase by the support surface, at least under the chosen deposition conditions, but leached during washing the sample with water. After 3–5 washing steps, the residual Cl content in the catalysts is close to the detection limit of XRF (50–110 ppm). This is equal to or even lower than the Cl content in the initial support.

Fig. 2 presents the transmission and diffuse reflectance UV–vis spectra used for identifying the gold state in the $Au/\delta\text{-}Al_2O_3$ catalyst (Table 1, DP-2 sample) at different stages of its preparation. The transmission spectrum of the $HAuCl_4$ + NaOH solution recorded immediately before its addition to the support (Fig. 2a) exhibits an absorption band centered at 48,000 cm^{-1}. Similar spectra with one weak ligand–metal charge transfer (LMCT) band at the UV region are characteristic of mononuclear complexes $[AuCl_2(OH)_2]^-$ and $[AuCl(OH)_3]^-$ that are formed by alkaline hydrolysis of $HAuCl_4$ [15]. According to Ref. [16], these complexes substitute their Cl and OH ligands for the surface OH groups of the support to form ≡**Al–**O–Au bonds. A subsequent repeated washing of the sample with warm water leads to the removal of gold ions weakly bound to the support and the hydrolysis of the Au–Cl bonds in the anchored complexes. In the diffuse reflectance UV–vis spectrum of the support after its interaction with a $HAuCl_4$ + NaOH solution followed by washing and drying (Fig. 2b), a broad absorption band is observed with a maximum at 44,000 cm^{-1}, which is likely due to the anchored gold hydroxide complexes. The large width of the absorption band indicates the non-uniform composition of the surface complexes, while shifting its maximum toward lower energies as compared to the spectrum of the $HAuCl_4$ + NaOH solution may be accounted for by the emergence of exchange coupling between gold ions upon their immobilization on the alumina surface [17]. The existence of exchange coupling indicates that the anchored metal complexes are associated, for example, collected in "islands" inside which metal ions are at a distance of about 0.5–1 nm from one another [18]. After calcination of the sample in air at 400 °C, an intense band centered at 19,000 cm^{-1} and a broad band in the region of 25,000–32,000 cm^{-1} appear instead of the 44,000 cm^{-1} band (Fig. 2c). The band at 19,000 cm^{-1} coincides with the most intense absorption band in the transmission UV–vis spectrum of a colloidal gold solution (Fig. 2d). Hence, the 19,000 cm^{-1} band in the spectrum of the $Au/\delta\text{-}Al_2O_3$ catalyst may be assigned to the plasmon absorption by metallic gold nanoparticles which are formed upon thermal decomposition of anchored gold hydroxide complexes.

The modeling of optical spectra of Au nanoparticles within the discrete dipole approximation supports the assignment [19]. The calculations demonstrate that, for uniform spherical gold particles

Table 1
Main characteristics of Au/Al_2O_3 samples (supports, Au and Cl contents, Au mean particle diameters), CO conversions (at GHSV = 60,000 h^{-1}) after different run times and steady-state reaction rates in CO oxidation at 40 °C.

Sample	Support	[Au] (wt.%)	$[Au]/[Au]_0$ (%)[a]	[Cl] (wt.%)	Average particle diameter (nm)[b]				CO conversion (%) at GHSV = 60,000 h^{-1} after		Reaction rate (mol s^{-1} g Au^{-1})[c]
					$\langle d_l \rangle$	$\langle d_{vs} \rangle$	$\langle d_m \rangle$	$\langle d_{XRD} \rangle$	1 h	7 h	
DP-1	δ-Al_2O_3	1.65[h]	82.5	~0.01	2.3 ± 0.9	3.3	4.3	≤3	91	92	0.280 (70)
DP-2	δ-Al_2O_3	1.45[i]	72.5	~0.01	2.7 ± 0.9	3.2	3.5	≤3	93	94	0.369 (77)
DP-3	γ-Al_2O_{3ms}	1.72[h]	86	~0.01	2.4 ± 0.7	2.8	2.9	≤3	88	88	0.192 (50)
DP-4	γ-Al_2O_{3ms}	1.34[i]	67	~0.01	6.4 ± 4.7[k]	12	13	≤3	19	31	0.037 (20)
DP-5	AOA-2	1.22[h]	61	~0.01	4.0 ± 1.3	5.0	5.8	≤3	60	58	0.104 (20)
IMP-1	γ-Al_2O_{3ms}	2.30	100	0.51	4.1 ± 0.9	4.4	4.6	≤3	<1	<1	<0.0005
IMP-1-1[d]	γ-Al_2O_{3ms}	2.29	100	~0.01	4.2 ± 1.0	4.6	4.9	≤3	77	77	0.086 (31)
IMP-2	δ-Al_2O_3	2.00	100	0.49	3.9 ± 1.5	5.1	5.9	≤3	<1	<1	<0.0005
IMP-3	δ-Al_2O_3	6.02	100	1.29	Polydispersed sample containing Au particles with d_i from 2 to 20 nm[l]			20	<1	<1	<0.0005
CLPG-1[e]	γ-Al_2O_{3ms}	3.8	81	~0.01	13.2 ± 2.8	14	15	12	<1	<1	<0.0005
CLPG-2[e]	γ-Al_2O_{3ms}	1.6	82	~0.01	n.m.			11	<1	<1	<0.0005
CVD-1[f]	γ-Al_2O_{3ms}	4.6[j] 1.4[j]	–	n.m.	Polydispersed sample containing Au particles with d_i from 2 to 20 nm[l]			n.m.	<1	<1	<0.0005
CVD-2[g]	γ-Al_2O_{3ms}	0.7	–	~0.01	3.3 ± 0.9	3.8	4.0		22	35	0.095 (20)

Reaction conditions: A flow reactor; catalyst weight, 40 mg; atmospheric pressure; feed stream composition: 1% CO, 20% O_2 and 2.4% steam in N_2; GHSV = 60,000–240,000 h^{-1}. DP, "deposition-precipitation"; IMP, impregnation; CLPG, "chemical liquid-phase grafting"; CVD, chemical vapor deposition; *ms*, microspherical; AOA-2, "active alumina" (see Section 2); n.m., not measured.

[a] Ratio between real and nominal Au content in the catalyst. Nominal gold content $[Au]_0$ is defined as follows: $[Au]_0 = [m_{Au}/(m_{Au} + m_{sup})] \times 100\%$, where m_{Au} and m_{sup} are the mass of gold and support taken for catalyst preparation.

[b] $\langle d_l \rangle = \Sigma d_i / \Sigma N$, $\langle d_{vs} \rangle = \Sigma d_i^3 / \Sigma d_i^2$ and $\langle d_m \rangle = \Sigma d_i^4 / \Sigma d_i^3$, where d_i, the Au particle diameter; N, the total number of particles observed; $\langle d_{XRD} \rangle$, average Au crystallite size calculated with Scherrer formula from Au(3 1 1) diffraction peak broadening.

[c] Degree of CO conversion (%) at which the reaction rate was determined is specified in parenthesis.

[d] The sample of IMP-1 after washing with 1 M NaOH.

[e] Prepared from $(CH_3)_2AuL$, where L = acetyl acetonate (CLPG-1) or dipivaloyl methanoate (CLPG-2).

[f] Prepared by passing $(CH_3)_2Au(acac)$ vapor through a fixed bed of the support.

[g] Prepared by treatment of the support with $(CH_3)_2Au(acac)$ vapor in a constantly rotating reactor.

[h] After five wash runs.

[i] After 10 wash runs.

[j] The upper number and lower one in the cell are the Au contents in the samples taken at the inlet and outlet parts of the sample bed, respectively.

[k] Bimodal particle size distribution with maxima at $d_1 = 3$ nm and $d_2 = 12$ nm.

[l] An accurate determination of the $\langle d_l \rangle$, $\langle d_{vs} \rangle$ и $\langle d_m \rangle$ values is impossible because of very wide particle size distribution and great numbers of very large Au crystals of irregular shape.

(monomers) of less than 30 nm in diameter (d_i), the maximum of plasmon absorption band (w_{max}) must be observed at 20,000 cm^{-1} in case the dielectric constant of the surrounding medium (ε_m) is close to 1, *i.e.* if the gold–support interaction is very weak. The position of the plasmon absorption band in the diffuse reflectance UV–vis spectrum of the Au/δ-Al_2O_3 catalyst ($w_{max} = 19,000\ cm^{-1}$) coincides with its position in the model spectrum calculated for

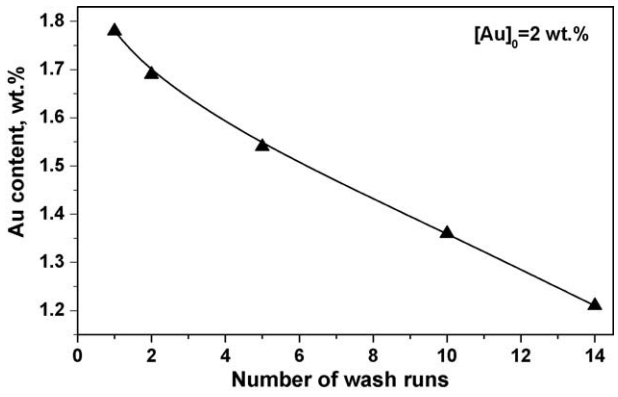

Fig. 1. Au content in the Au/γ-Al_2O_{3ms} catalyst prepared by the "deposition-precipitation" method in dependence on the number of water washing steps. $[Au]_0$ stands for the nominal gold content in the samples ($[Au]_0 = [m_{Au}/(m_{Au} + m_{sup})] \times 100\%$, where m_{Au} and m_{sup} are the mass of gold and support taken for catalyst preparation, respectively).

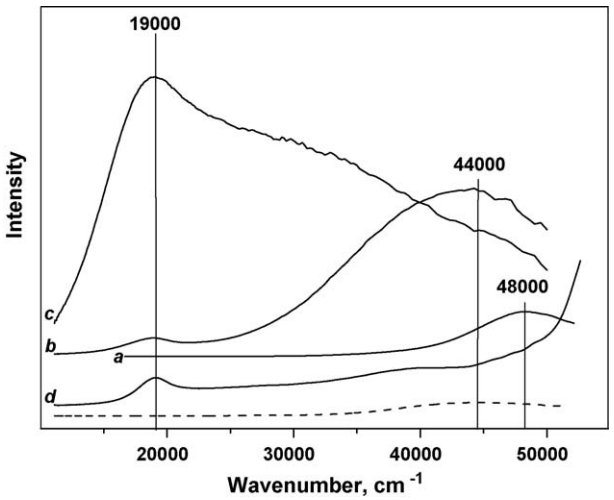

Fig. 2. Transmission (a and d) and diffuse reflectance (b and c) UV–vis spectra of (a) an aqueous $HAuCl_4$ + NaOH solution ($C_{Au} = 0.013$ M, $C_{OH}/C_{Au} = 3.8$ mol/mol), (b) the δ-Al_2O_3 support after adsorption of Au complexes from solution *a*, repeated washing with water and drying, (c) sample *b* after calcination in air at 400 °C for 4 h (Table 1, DP-2 sample), and (d) an aqueous solution of colloidal gold ($C_{Au} = 2.5 \times 10^{-4}$ M, mean diameter of Au particles is *ca.* 50 nm). The diffuse reflectance UV–vis spectrum of initial δ-Al_2O_3 is shown by the dashed line.

ε_m = 2.3. The fact that this value is close to ε_m = 3.0–3.3 obtained from the experimental refractive indexes for bulk alumina allows the existence of some decoration of Au particles by the support to be supposed [20].

The broad absorption band in the region of 25,000–32,000 cm^{-1}, which is also seen in the diffuse reflectance UV–vis spectrum of the Au/δ-Al_2O_3 catalyst, cannot arise from metallic gold since in no case can the plasmon absorption band be shifted so far toward higher energies [21]. Its assignment to the *d*–*d* transitions of gold cations is also excluded because of its high intensity, which is comparable to the intensities of LMCT bands in the spectra of metal complexes. On the other hand, similar bands were observed in the diffuse reflectance UV–vis spectra of copper-containing oxide (CuO–MgO, Cu–ZnO–Al_2O_3) and zeolite (CuY, Cu-ZSM-5) catalysts and assigned to square-planar copper clusters with bridging oxygen [22]. By analogy, we assumed that the 25,000–32,000 cm^{-1} band in the diffuse reflectance UV–vis spectrum of the Au/δ–Al_2O_3 catalyst is assigned to Au clusters with bridging oxygen ions that are located on the support surface together with metallic Au nanoparticles. The DFT calculations [19] show that the electronic spectra of square-planar complexes $[AuX(\mu_2\text{–}O)(H_2O)]_n$ (X = Cl or OH) must contain two strong overlapped absorption bands with maxima at 26,000 and 30,000 cm^{-1}, each consisting of several discrete transitions caused by electron density transfer from ligands of the first coordination sphere to Au ions and from Au ions to the bridging oxygen atoms. This result can be considered as evidence for that the 25,000–32,000 cm^{-1} band in the diffuse reflectance UV–vis spectra of the Au/Al_2O_3 catalysts corresponds to the surface "ionic" Au species with bridging oxygen.

In our opinion, polynuclear gold species with Au–O–Au bonds can form, for example, early in the catalyst calcination due to intermolecular condensation of the "outer" OH ligands of the anchored Au hydroxide complexes located in the close proximity to each other to eliminate water molecules. Upon further heating, the surface Au oxide species decompose to form the metallic nanoparticles, while a part of them are thought to preserve even after long-term calcination of the sample in air at 400 °C.

XRD patterns of uncalcined Au/Al_2O_3 samples prepared by DP exhibit only diffraction peaks from γ- or δ-Al_2O_3. It suggests that the anchored Au hydroxide complexes exist in the molecular dispersed state or as the clusters ("islands") of no more than 3–4 nm in size. Upon calcining the samples in air at 400 °C, weak, broadened peaks related to Au metal appear in the XRD patterns. Since the most intense Au(1 1 1), Au(2 0 0) and Au(2 2 0) peaks are superposed on the peaks from the Al_2O_3 phase, the Au (3 1 1) peak which is not superposed on any of Al_2O_3 peaks can be used for determination of the sizes of Au crystallites. However, in the case of the Au/Al_2O_3 catalysts prepared by DP, this peak usually is strongly broadened (Fig. 3a), so its width cannot be measured with sufficient accuracy. We can only assert that the average size of Au crystallites is no more than 3 nm in the catalysts thus prepared.

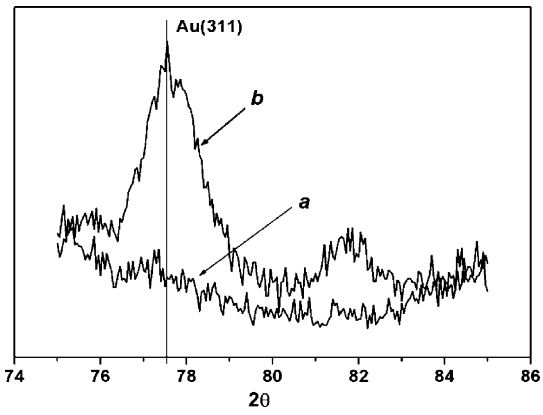

Fig. 3. Fragments of XRD patterns of Au/γ-Al_2O_{3ms} catalysts prepared by the "deposition-precipitation" (a) and "chemical liquid-phase grafting" (b) methods (Table 1, DP-4 and CLPG-1 samples, respectively) in the region of Au(3 1 1) peak.

To estimate the sizes of metal particles in the nanodispersed Au catalysts more definitely we used an electron microscopy. TEM micrographs taken with a medium magnification demonstrate contrast images of near-spherical Au particles, which are evenly distributed over the support surface (see Fig. 4a as an example). However, due to the peculiarities of diffraction contrast in the bright-field images, the most dispersed Au particles are almost invisible against the Al_2O_3 background during conventional bright-field imaging in the TEM mode (Fig. 5a). If any doubt arose as to whether a visible object is an Au particle or a fragment of Al_2O_3 particle, the same region of the sample surface was imaged in the high-angle dark-field (HADF) mode. After switching to HADF mode, Au particles are imaged as bright spots and can be discerned more definitely (Fig. 5b). Results of measuring diameters of Au particles seen in TEM micrographs were used for determination of

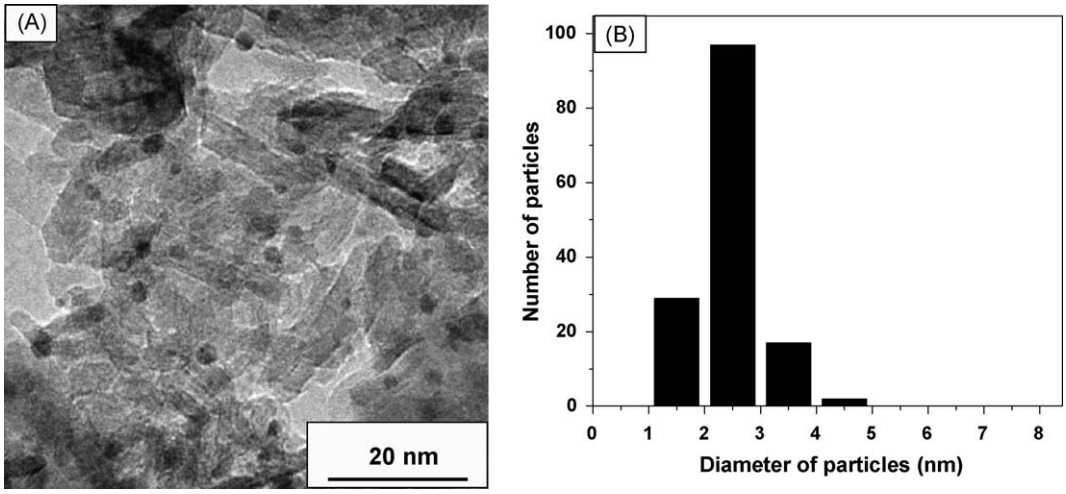

Fig. 4. TEM image (A) and Au particle size distribution (B) of the 1.7% Au/γ-Al_2O_{3ms} catalyst prepared by the "deposition-precipitation" method and calcined in air at 400 °C (the time period between drying and calcining the sample was 1 day). The average diameters of Au particles calculated from the histogram are given in Table 1 (DP-3 sample).

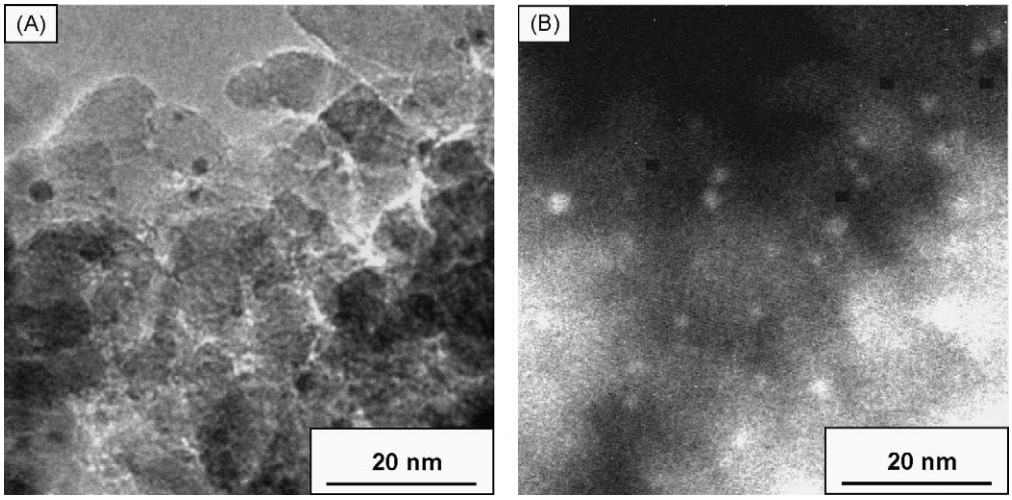

Fig. 5. Bright-field (A) and high-angle dark-field (HADF) (B) TEM images of a region of the 1.5% Au/δ-Al_2O_3 catalyst prepared by the "deposition-precipitation" method and calcined in air at 400 °C. The average diameters of Au particles are given in Table 1 (DP-2 sample).

particle size distributions. From 150 to 500 crystals were included in the distribution for each sample. Average diameters of Au particles were calculated from the particle size distributions by formulas specified in the footnote to Table 1.

From TEM data, the Au/Al_2O_3 catalysts prepared by the standard DP procedure (Table 1, DP-1, DP-2 and DP-3 samples) contain mainly Au particles of 2–4 nm in diameter. Besides, few larger Au particles (d_i = 5–8 nm) are seen. Particle size distributions closely match a lognormal shape with the maximum between 2 and 3 nm (Fig. 4b). The lognormal shape of particle size distribution allows us to suggest that metallic Au particles arise through the process of migration and subsequent coalescence of the "primary" metal crystallites [23], which are formed during the thermal decomposition of anchored Au complexes.

The elongation in the period between sample drying and calcination from 1 to 2 days to several weeks results in the appearance of large Au particles of up to 20 nm in size (Table 1, DP-4 sample). As a result, the particle size distribution of Au particles in this case has a bimodal shape with maxima at 4 and 12 nm (Fig. 6). Meanwhile, the average size of Au crystallites ($\langle d_{XRD} \rangle$) is no more than 3 nm, as estimated from the width of Au(3 1 1) reflection, *i.e.* the contribution of relatively large metal particles into the broadening of the diffraction peak is not noticeable. High-resolution (HR) TEM study of this sample reveals that many of Au particles of ≥6 nm in size consist of several twined crystallites, each 3–5 nm in size (an example of the multiple twined Au particle is shown in Fig. 7). It seems like that such substructure of medium- and large-sized Au particles causes the discrepancy between TEM and XRD data in the case under consideration. Comparing the TEM and XRD data presented in Table 1, it is easy to see that for the Au/Al_2O_3 catalysts prepared by DP the average sizes of Au particles determined by TEM exceed that estimated from XRD data ($\langle d_{XRD} \rangle \leq 3$ nm). This fact indicates that the formation of multiple twined Au particles from monodisperse metallic crystallites is typical of the Au/Al_2O_3 catalysts prepared by DP. It also follows that XRD estimation of the size of Au crystallites in these catalysts may be understated and needs TEM control.

3.1.2. Catalysts prepared by impregnation

The possibility of preventing gold losses during the catalyst preparation makes the impregnation technique very attractive. Fig. 8 shows the transmission and diffuse reflectance UV–vis spectra recorded in the course of preparation of the impregnated 2.3% Au/γ-Al_2O_{3ms} catalyst (Table 1, IMP-1 sample). The transmission spectrum of an aqueous $HAuCl_4$ solution used for impregnating the support (Fig. 8a) exhibits strong LMCT bands at 31,800

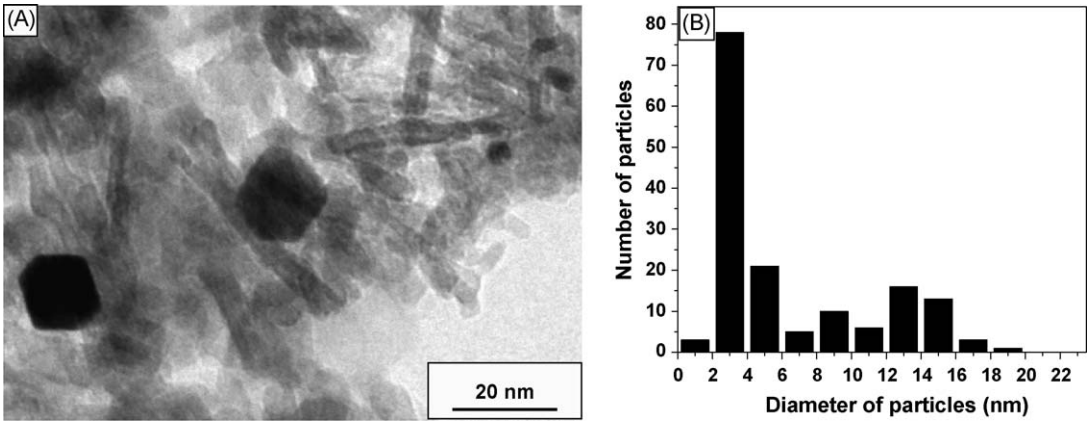

Fig. 6. TEM image (A) and Au particle size distribution (B) of the 1.3% Au/γ-Al_2O_{3ms} catalyst prepared by the "deposition-precipitation" method and calcined in air at 400 °C (the time period between drying and calcining the sample was 2 weeks). The average diameters of Au particles calculated from the histogram are given in Table 1 (DP-4 sample).

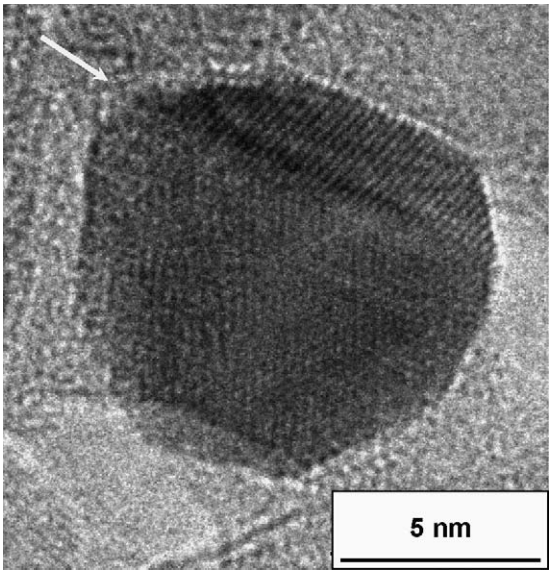

Fig. 7. HRTEM image of the Au particle with a diameter of *ca.* 11 nm located at the surface of the 1.3% Au/γ-Al_2O_{3m} catalyst (Table 1, DP-4 sample). The shape defects (twin dislocations) are seen implying that the particle is composed of several smaller crystallites (multiple twinning). The arrow indicates the (1 1 1) twin boundary.

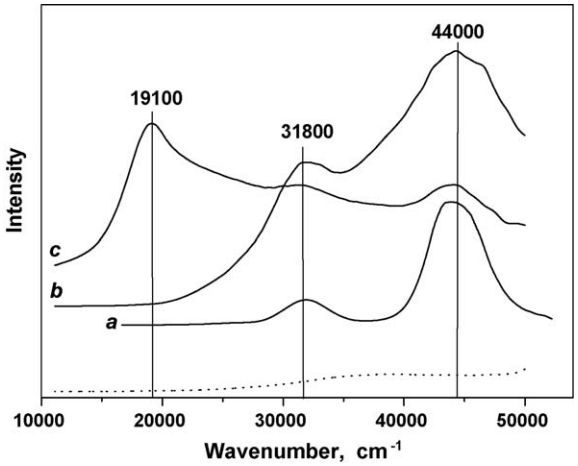

Fig. 8. Transmission (a) and diffuse reflectance (b and c) UV–vis spectra of (a) an aqueous $HAuCl_4$ solution (C_{Au} = 0.085 M), (*b*) the γ-Al_2O_{3ms} support after impregnation with solution *a* and drying, (c) sample *b* after reduction with H_2 at 400 °C for 4 h (Table 1, IMP-1 sample). The diffuse reflectance UV–vis spectrum of initial γ-Al_2O_{3ms} is shown by the dashed line.

and 44,000 cm^{-1} belonging to $[AuCl_4]^-$ complexes [17]. The same bands, but somewhat broadened, appear in the diffuse reflectance UV–vis spectrum of γ-Al_2O_3 after impregnation with the $HAuCl_4$ solution (Fig. 8b). Subsequent treatment of the '$HAuCl_4$'/γ-Al_2O_{3ms} sample with H_2 at 400 °C leads to the appearance of the strong band at 19,000–19,500 cm^{-1} derived from the plasmon absorption by metallic gold nanoparticles (Fig. 8c). Simultaneously, the absorption bands at 31,800 and 44,000 cm^{-1} considerably weaken but do not totally disappear from the spectrum. It suggests that, even after a long-term treatment of '$HAuCl_4$'/γ-Al_2O_{3ms} sample with H_2 at high temperature, only a part of supported Au^{III} chloride complexes have been reduced. This is consistent with the XRF data that the IMP-1 sample treated with H_2 contains a considerable amount of residual Cl (*ca.* 5000 ppm). One can hardly say if the gold complexes with bridging oxygen, like those detected in the DP catalysts, occur in the impregnated samples, since the LMCT bands of these complexes in the region of 25,000–32,000 cm^{-1} may be masked by the absorption of Au^{III} chloride complexes.

XRD patterns of the samples prepared by impregnation of γ- and δ-Al_2O_3 with the $HAuCl_4$ solution and containing *ca.* 2 wt.% Au (Table 1, IMP-1 and IMP-2 samples) resemble diffraction patterns of highly dispersed DP catalysts. It is also impossible to determine precisely the Au crystallite size due to very strong broadening of diffraction peaks. From the TEM data (Table 1 and Fig. 9), IMP-1 and IMP-2 samples comprise both small ($d_i < 5$ nm) and relatively large (d_i = 7–10 nm) Au particles, while the former predominate in the number and weight fraction. Particle sizes of both samples are fitted well by the lognormal distribution with the maximum at $d_i \approx 4$ nm. For IMP-1 and IMP-2 samples, the mass-averaged diameters of Au particles ($\langle d_m \rangle$ = 4.6 and 5.9 nm, respectively) determined by TEM noticeably exceed the Au crystallite size ($\langle d_{XRD} \rangle \leq 3$ nm). Hence, the larger Au particles in the impregnated samples are supposed to be multiple twined ones like the Au particles in the catalysts prepared by DP.

Thus, contrary to the widespread opinion [24–27], our observations show that the conventional impregnation technique with the use of $HAuCl_4$ as precursor allows obtaining the Au/Al_2O_3 samples exhibiting the supported gold dispersion which is almost as high as that for the catalysts prepared by DP. However, one should keep in mind that the Au dispersion in the impregnated

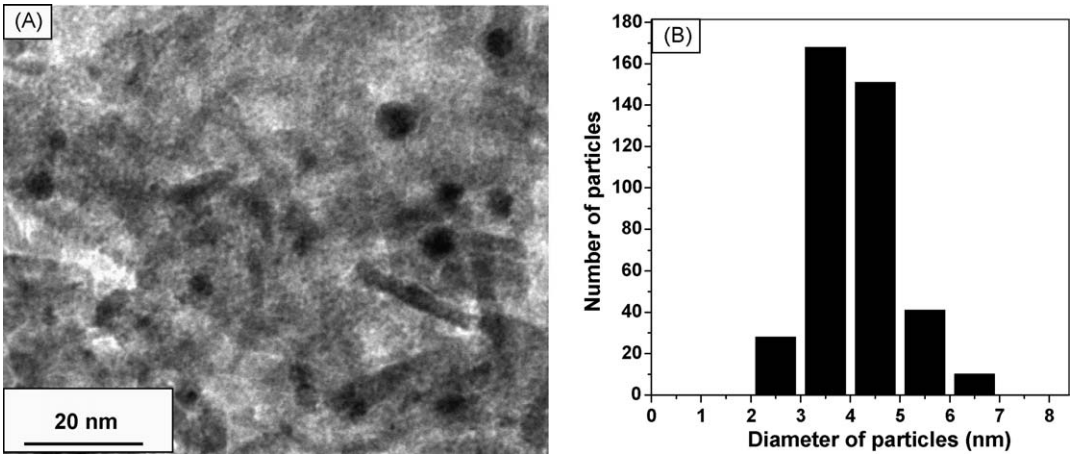

Fig. 9. TEM image (A) and Au particle size distribution (B) of the 2.3% Au/γ-Al_2O_{3ms} catalyst prepared by the impregnation method and reduced with H_2 at 400 °C. The average diameters of Au particles calculated from the histogram are given in Table 1 (IMP-1 sample).

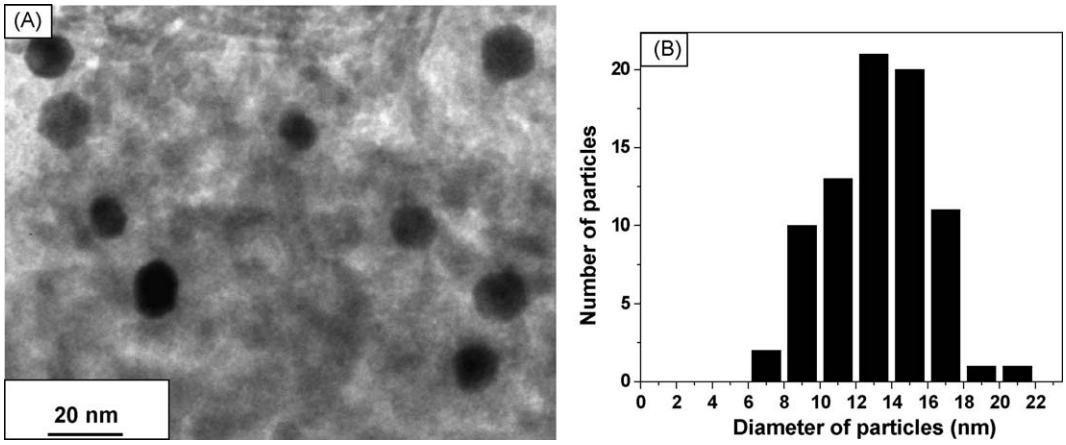

Fig. 10. TEM image (A) and Au particle size distribution (B) of the 3.8% Au/γ-Al_2O_{3ms} catalyst prepared by the 'chemical liquid-phase grafting' method and calcined in air at 400 °C. The average diameters of Au particles calculated from the histogram are given in Table 1 (CLPG-1 sample).

samples decreases with an increase in the supported metal loading. Indeed, the sample containing 6 wt.% of Au on δ-Al_2O_3 (Table 1, IMP-3 sample) comprises, apart from small Au particles (d_i = 2–5 nm), numerous large particles with the sizes ranging from 6 to 50 nm. For this sample, an accurate determination of the average diameters of Au particles from TEM data is impossible because of very broad particle size distribution and great numbers of very large particles of irregular shape. The Au crystallite size determined by XRD for IMP-3 sample is 24 nm (as calculated from the width of Au(2 2 0) and Au(2 2 2) reflections) or 20 nm (from the width of Au(3 1 1) reflection) that is three to four times larger than the mass-averaged diameter of Au particles for IMP-1 and IMP-2 samples containing 2 wt.% Au.

The observed effect can be interpreted based on the results obtained in experiments when the samples of δ-Al_2O_3 impregnated with an acidic $HAuCl_4$ solution at 25 °C were repeatedly washed with distilled water, dried and then analyzed for the residual Au content [28]. It was established that the impregnation of δ-Al_2O_3 with the $HAuCl_4$ solution is accompanied by strong adsorption of Au^{III} chloride complexes on the support surface, the amount of the chemically adsorbed Au species which are not leached with water depending only slightly on the concentration of impregnating solution within the range of 0.075–0.250 M. As a consequence, the impregnated '$HAuCl_4$'/δ-Al_2O_3 samples with the nominal Au loading of 2 and 6 wt.% after their washing with water contain 1.5 and 1.8 wt.% Au, respectively. Thus, one can assert that the samples of '$HAuCl_4$'/Al_2O_3 with a low (≤2 wt.%) content of gold contain mainly the covalently anchored Au^{III} complexes that are formed, for example, by substitution of one or two ligands from $[AuCl_4]^-$ and $[Au(OH)Cl_3]^-$ complexes, which dominate in strongly acidic $HAuCl_4$ solutions [15], by the equivalent number of OH groups on the support surface. At higher Au loading, the '$HAuCl_4$'/Al_2O_3 sample must comprise, apart from molecular-level dispersed "islands" of anchored complexes, a considerable amount of $(H_3O)AuCl_4{\cdot}xH_2O$ crystals which are physically retained inside the support pores. Obviously, the share of weakly bound gold species should increase with an increase in the Au loading. While a sharp decrease in the Au dispersion on Al_2O_3 is observed with an increase in the total Au loading, it is reasonable to suppose that nanodispersed Au^0 particles are formed upon reduction of the chemically anchored Au complexes and the coarse metal particles are resulted from weakly bound $(H_3O)AuCl_4{\cdot}xH_2O$ crystals. The above consideration leads to conclude that the conventional impregnation technique can hardly produce Au/Al_2O_3 materials bearing high Au dispersion at the high metal loading. However, the impregnation procedure may be appropriate for preparation of nanodispersed Au/Al_2O_3 catalysts with a low (<2 wt.%) content of the noble metal.

3.1.3. Catalysts prepared by CLPG

As a result of interaction between γ-Al_2O_{3ms} and $(CH_3)_2AuL$ in *n*-pentane solution, the amount of gold deposited reaches 80–85% of the total amount of gold contained in the solution (Table 1, CLPG-1 and CLPG-2 samples). However, it should be kept in mind that the CLPG procedure does not provide for sample washing with a pure solvent and, therefore, the resulted samples may contain the complexes which are only physically adsorbed without chemical bonding to the support. Upon heating in air, a part of the deposited complexes are vaporized from the support surface and the rest are decomposed with the formation of metallic gold. The gold lost caused by the vaporization of $(CH_3)_2AuL$ complexes can be fully excluded by placing the sample in a furnace pre-heated to temperatures above 400 °C (fast thermolysis) at which decomposition of the supported complexes proceeds much faster than their vaporization. XRF analysis of the samples prepared by CLPG indicates very low Cl content of 100–200 ppm that is comparable to the Cl level in the initial γ-Al_2O_{3ms} support.

XRD patterns of CLPG-1 and CLPG-2 samples exhibit the relatively narrow and symmetrical Au(3 1 1) peak (Fig. 2b) that allows the Au crystallite sizes to be determined at a good accuracy. For these samples, the value of $\langle d_{XRD}\rangle$ depends only slightly on the Au loading at least within the range of 1–4 wt. % Au and is equal to 11–12 nm. From TEM data (Fig. 10), the CLPG-1 sample contains Au particles with d_i values ranging from 7 to 20 nm, the value of $\langle d_m\rangle$ calculated from the TEM histogram being close to the $\langle d_{XRD}\rangle$ value determined for this sample (see Table 1). The latter suggests that Au particles contained in the CLPG-1 sample are monocrystalline unlike that observed for the catalysts prepared by the DP or impregnation techniques. The absence of particularly small ($d_i < 5$ nm) Au particles in the Au/Al_2O_3 samples prepared by CLPG may result from the fact that $(CH_3)_2AuL$ complexes interact less strongly with the alumina surface than Au chloride or hydroxide complexes and, in addition, possess high saturated vapor pressure at relatively low temperatures. For these reasons, the deposited organogold complexes may migrate during calcination both over the support surface and through gas phase towards sites of anchoring of the growing $[(CH_3)_2AuL]_n$ "islands" as nuclei of coarse metal particles.

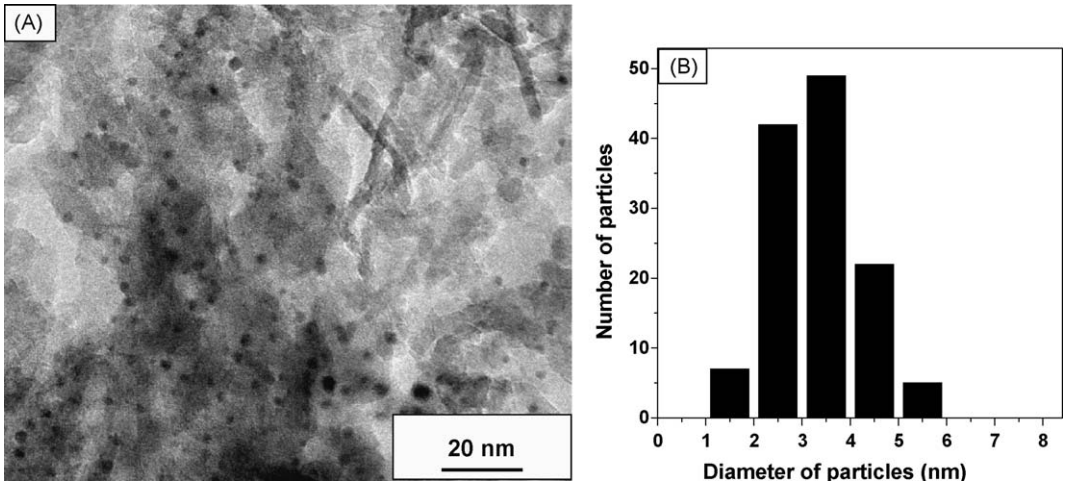

Fig. 11. TEM image (A) and Au particle size distribution (B) of the 0.7% Au/γ-Al_2O_{3ms} catalyst prepared by the chemical vapor deposition method in a constantly rotating reactor and calcined in air at 325 °C. The average diameters of Au particles calculated from the histogram are given in Table 1 (CVD-2 sample).

3.1.4. Catalysts prepared by CVD

As a gold complex is supported from its solution in an organic solvent, the solvent molecules can adsorb on the support surface and hinder the interaction between the complex and functional groups of the support [11]. The problem can be avoided by supporting volatile gold compounds from gas phase.

When $(CH_3)_2$Au(acac) vapor was passed through a fixed bed of γ-Al_2O_{3ms} at 25 °C, the complex partially decomposed under the action of molecular adsorbed water remained on the support surface, as indicated by the characteristic change of vapor color. After calcination in air at 325 °C, the sample became brownish-violet colored that indicated the formation of metallic Au nanoparticles. Chemical analysis of the sample specimens taken from various parts of the reactor (Table 1, CVD-1 sample) showed that the Au content decreased along the support layer in the direction of the gas flow.

To prevent uncontrollable decomposition of the precursor and provide uniform distribution of the deposited component along the support layer, we modified the CVD procedure. First, the temperature of pre-dehydration of alumina in vacuum (ca. 10^{-5} Pa) was elevated up to 300–350 °C; second, treatment of the support with the complex vapor was conducted under quasi-static conditions using a continuously rotated reactor. The samples thus prepared were uniformly colored, and analysis of several specimens of the same sample for the Au content gave almost the same results.

According to TEM data (Table 1), the CVD-1 sample prepared by passing $(CH_3)_2$Au(acac) vapor through the fixed bed of γ-Al_2O_{3ms} contains Au particles ranging in diameter between 5 and 35 nm. Gold particles of <20 nm in size are spherical, while larger particles are oval (from 25 to 125 nm in length and up to 85 nm in cross-dimension) and not faceted. TEM images of the samples prepared in a constantly rotating reactor (see Fig. 11A as an example) show microaggregates of the primary γ-Al_2O_3 globules which are mainly covered with small Au particles of 2–4 nm in diameter. In addition, some larger particles with d_i = 5–10 nm are seen. Generally, the particle size distributions for the samples thus prepared are rather narrow with the maximum between 2.5 and 3.0 nm, as shown in Fig. 11B. HPTEM images obtained with the CVD-2 sample show several Au nanocrystals to be close to ideal polyhedrons in shape. At the same time, the structure of many Au particles is far from perfect and contains numerous defects (twin boundaries, corners, steps, *etc.*) and close packed planes with the increasing number of surface exposed atoms (Fig. 12A). Along the edges of the HRTEM images of some Au particles with defect-rich surface, the surface exposed Au atoms of low coordination are seen, as illustrated in

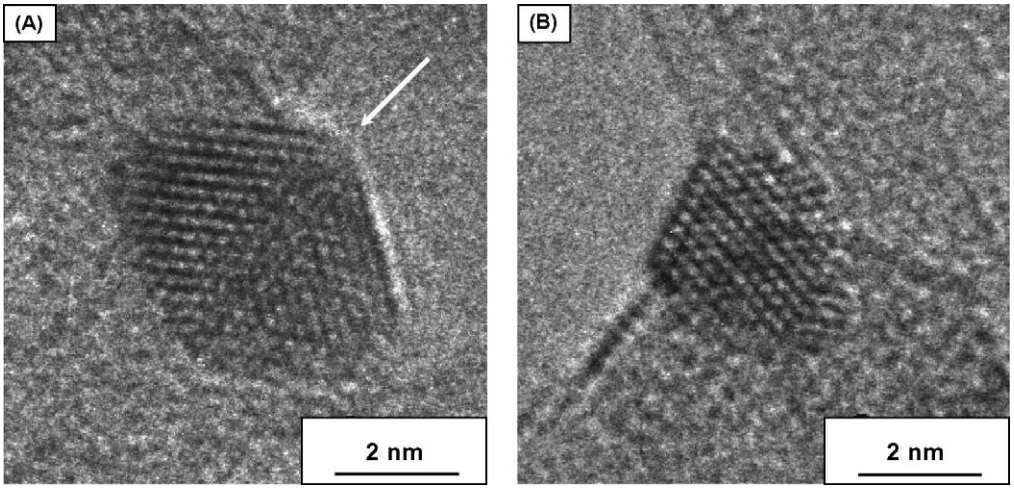

Fig. 12. HRTEM images of the defect-rich Au particles with diameters of 4.5 nm (A) and 2.6 nm (B) which are located at the surface of the 0.7% Au/γ-Al_2O_{3ms} catalyst prepared by the chemical vapor deposition method and calcined in air at 325 °C (Table 1, CVD-2 sample). The arrow indicates the (1 1 1) twin boundary.

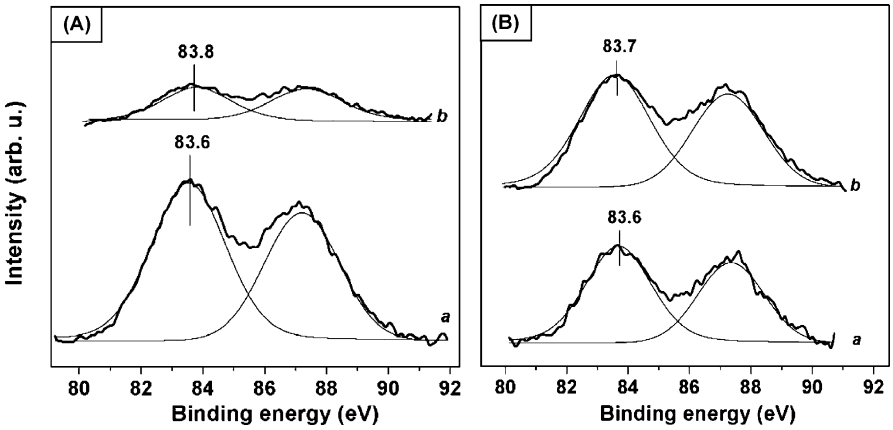

Fig. 13. XP Au 4f spectra of the 0.7% Au/γ-Al_2O_{3ms} catalyst prepared by the chemical vapor deposition (A) and the 1.5% Au/δ-Al_2O_3 catalyst prepared by the 'deposition-precipitation' (B) methods. The catalyst samples were taken for the spectra measuring both (a) as prepared and (b) after grinding in an agate mortar. The average diameters of Au particles are presented in Table 1 (CVD-2 and DP-2 samples, respectively).

Fig. 12B. Some authors [2,29] believe that the similar low-coordinated Au atoms (or their ensembles) on the metal crystallite surface are the sites for binding CO and, perhaps, oxygen (O atoms and/or O_2 molecules) during CO oxidation.

3.2. Penetration depth of gold into the support granule in the Au/Al_2O_3 catalysts prepared by various techniques (from XPS data)

The survey XP spectra of the Au/Al_2O_3 samples prepared by various techniques contain the core level peaks which are characteristic of alumina (the Al 2p and O 1s peaks at 74.5 and 531.6 eV, respectively), gold (the Au 4f peak) and hydrocarbon impurities (the C 1s peak at 284.6 eV). In addition, the spectra of the samples prepared by the impregnation technique exhibit the distinct Cl 2p peak at 198.7 eV derived from Cl^- ions. In the spectra of the samples prepared by other methods, the intensity of this peak is at the noise level.

Fig. 13 shows the typical Au 4f core level spectra measured from the Au/Al_2O_3 samples. In all the cases the spectra are fitted well by a single doublet line consisting of the Au $4f_{7/2}$ and Au $4f_{5/2}$ peaks that appeared as a result of a spin–orbital splitting. Only binding energies corresponding to the more intense Au $4f_{7/2}$ peak are used for the following discussion. The E_b(Au $4f_{7/2}$) values as well as the Au/Al and Cl/Al atomic ratios measured for the Au/Al_2O_3 samples prepared by various methods are given in Table 2. According to the data obtained, the value of E_b(Au $4f_{7/2}$) remains practically constant upon varying the sample preparation technique or the Au dispersion (at least when the $\langle d_l \rangle$ value is changed between 3 and 30 nm) and is equal to 83.6 ± 0.2 eV. Such a E_b(Au $4f_{7/2}$) value is typical of metallic gold particles supported on various oxide carriers [30]. The fact that no peaks are observed in the E_b region of 84.5–88 eV characteristic of "ionic" gold species can be accounted for by the rapid reduction of Au^{III} or Au^{I} species, if any are contained in the sample, under the action of photoelectron beam during recording the XP spectra [7].

Fig. 13A demonstrates that the intensity of the Au $4f_{7/2}$ peak (I_{Au}) in the XP spectrum of the Au/γ-Al_2O_{3ms} catalyst prepared by CVD strongly depends on the degree of sample grinding before the spectrum registration. Grinding the sample in an agate mortar to powder with particles of 2–5 μm in size causes a significant decrease in the I_{Au} value and corresponding decrease in the determined Au/Al atomic ratio (which is calculated from I_{Au} normalized on the Al 2p peak area), while the E_b(Au $4f_{7/2}$) value practically does not change at that. A similar, but less considerable though, decrease in the I_{Au} and Au/Al values also is observed as a result of grinding the samples prepared by CLPG, the value of E_b(Au $4f_{7/2}$) again being practically unchanged (Table 2).

TEM analysis of the grinded CLPG-2 and CVD-2 samples does not show changes in the diameters of supported Au particles as compared with those for the non-grinded specimens of the same samples. Hence, sintering of particles (for example, due to local overheating during grinding) cannot be the reason for relatively low intensity of the peaks in the Au 4f core level spectra of the grinded samples. It is most likely that the effect observed is accounted for by low depth of Au penetration into the support granules. Upon grinding the sample, internal surface of Al_2O_3 granules becomes exposed and, therefore, a decrease in the intensity of the XP peak of metallic gold, which is observed in the spectrum of grinded sample as compared with that for the non-grinded specimen of the same sample, argues for the predominant gold localization on the external surface of support granules (the "egg shell" type of distribution of the supported component).

The data of Table 2 and Fig. 13B show that the Au/Al atomic ratios determined by XPS coincide for the grinded and non-grinded specimens of the same sample prepared by the DP or impregnation techniques within the limits of experimental error (±0.001). This indicates rather uniform gold distribution between the external and internal surfaces of the support granules. It is not clear yet why the use of $(CH_3)_2$AuL as the gold metal precursor causes less uniform

Table 2
The Au $4f_{7/2}$ binding energies, Au/Al and Cl/Al atomic ratios obtained by XPS for the Au/Al_2O_3 catalysts prepared by various techniques.

Sample[a]	$\langle d_l \rangle$ (nm)[b]	E_b(Au $4f_{7/2}$) (eV)[c]	Atomic ratios[c]	
			Au/Al[d]	Cl/Al[d]
DP-2	2.7	83.6 (83.7)	0.004 (0.005)	≤0.001
DP-4	6.4	83.7 (83.6)	0.003 (0.002)	0.007 (0.006)
IMP-1	4.1	83.8 (83.8)	0.004 (0.005)	0.028 (0.043)
CLPG-1	13.2	83.6 (83.5)	0.007 (0.004)	≤0.001
CVD-1	20–25	83.6 (n.m.)	0.004 (n.m.)	≤0.001
CVD-2	3.3	83.6 (83.8)	0.010 (0.002)	≤0.001

DP, "deposition-precipitation"; IMP, impregnation; CLPG, "chemical liquid-phase grafting"; CVD, chemical vapor deposition; E_b(Au $4f_{7/2}$), the Au $4f_{7/2}$ binding energy; n.m., not measured.

[a] The chemical composition of the samples is presented in Table 1.

[b] The average Au particle diameter calculated from the TEM histograms (see Table 1).

[c] The values measured for the samples grinded in an agate mortar are given in parenthesis.

[d] Calculated from the integrated intensities of the Au $4f_{7/2}$, Al 2p and Cl 2p peaks using the corresponding atomic sensitivity factors taken from Ref [14].

metal distribution through the volume of the catalyst granule than the use of Au chloride or hydroxide complexes. Perhaps, gold complexes containing bulky organic ligands hardly penetrate into narrow pores of the support and concentrated at its external surface during the deposition procedure.

3.3. Catalytic activity of Au/Al_2O_3 catalysts in CO oxidation in excess dioxygen

3.3.1. Catalytic behavior during combustion of CO (1 vol.%) in a wet airflow at 40 °C

The activities of the Au/Al_2O_3 catalysts prepared by different methods were compared under the reaction conditions simulating the cleaning of a wet airflow (flow rate 6–24 l/h) from CO impurity (1 vol.%) at the temperature (40 °C) little higher than ambient temperature. The results are summarized in Table 1.

Under given conditions, the catalysts prepared by DP and containing mainly small Au particles with the volume-surface average particle diameter ($\langle d_{vs}\rangle$) of ≤5 nm exhibit extraordinary high activity for CO oxidation, the CO conversion being not significantly changed during the whole testing run (typically, for 7–8 h). Over the most active DP-1 and DP-2 catalysts prepared by deposition of gold onto δ-Al_2O_3, the CO conversion reached 70–77% even at the contact time (τ) of 0.015 s (GHSV = 240,000 h^{-1}) that was the minimum τ value possible during our testing procedure. That did not allow the inlet and outlet CO and CO_2 contents to be measured under differential conditions and, therefore, the reaction rates presented in Table 1 for these catalysts are somewhat understated. The DP-4 catalyst wherein the Au particles have a bimodal particle size distribution within the range of 2–20 nm was significantly less active than the DP-1, DP-2 and DP-3 catalysts containing only relatively small metal particles ($\langle d_{vs}\rangle \leq 5$ nm).

The catalysts prepared by the CLPG technique demonstrate very low activities in CO oxidation. In the presence of these catalysts the traces of CO_2 are only detected in the outlet gas upon temperature increasing up to 300 °C, the CO conversion being as low as *ca.* 2%. Since the volume-surface or mass-averaged diameters of Au particles determined for the CLPG-1 sample by TEM are not too far from those of the DP-4 sample, the observed dramatic difference in the catalytic activity could be attributed to different shapes of Au particle size distributions of these two samples. Comparison between Figs. 6B and 10B reveals that the DP-4 sample has the wide Au particle size distribution encompassing particles with diameters in the range from 3 to 20 nm, whereas the particle size distribution of the CLPG-1 sample is much narrower and includes virtually no Au particles less than 5 nm in diameter.

This suggests the same dependence of the CO oxidation activity on the size of Au particles for the Au/Al_2O_3 catalysts as the dependence discovered previously for Au catalysts with other support materials (TiO_2, Co_3O_4 or α-Fe_2O_3) [26,31], *viz.* the catalytic activity expressed in terms of turnover frequency (TOF) increases sharply (by several orders of magnitude) with a decrease in the Au particle size down to 2–3 nm. This is a specific feature of Au catalysts for CO oxidation that makes them different from, for example, Pt or Rh catalysts whose activity (in terms of TOF) either decreases with an increase in or does not depend on the metal particle size [32–34]. The question why a decrease of Au particles in size results in a sharp increase in their catalytic activity in the CO + O_2 reaction is still disputed in spite of the numerous efforts to answer it. The most common explanations are that the reactants (CO, O_2, O) may interact only with low-coordinated Au atoms on the surface of metal particles, which rapidly increase in number with decreasing Au particle size [29], or with small (2 atoms thick) Au clusters, which are characterized by a rather wide band-gap (quantum-size effect) [35]. Some researchers suppose that anion vacancies [7] or OH groups [7,36] of the support surface take part in the catalytic cycle of CO oxidation and, consequently, the active sites are located at the interface between the Au particle and the support surface. Hence, the number of the active sites should be in direct proportion to the interface length l_i which is, in turn, inversely proportional to d_i^2.

The Au/γ-Al_2O_{3ms} catalyst prepared by impregnation of the support with a $HAuCl_4$ solution followed by reduction with H_2 at 400 °C (Table 1, IMP-1 sample) exhibits no activity in low-temperature CO oxidation, even though it contains a large fraction number of Au particles with $d_i < 5$ nm. Probably, the lack of catalytic activity in the given case is caused by a large content of chloride ions in the sample. According to the mechanistic concepts developed in some recent contributions [37,38], chlorides may bind to Au^{x+} cations that are part of the active sites of Au catalysts for CO oxidation and thus prevent the formation of Au–OH species playing a key role in the catalytic cycle which will be discussed below in some more details. However, as seen from Table 1, the IMP-1 sample can be activated by washing with an aqueous 1 M NaOH solution. This procedure leads neither to gold leaching from the sample nor to changes in the average size of Au particles, but allows the Cl content to be decreased by an order of magnitude. As soon as the chloride anions are eliminated, the activity of the impregnated sample in the CO + O_2 reaction becomes comparable to the activity of catalysts prepared by the DP technique and containing Au particles with the average diameter approximately equal to that for the impregnated catalyst ($\langle d_{vs}\rangle$ = 4–5 nm).

Testing the catalytic activity of the Au/γ-Al_2O_{3ms} samples prepared by CVD (Table 1, CVD-1 and CVD-2 samples) also provides evidence of the size effect. The CVD-1 sample, which contained only Au particles at least 5 nm in diameter, does not show any pronounced activity in CO oxidation at 40 °C. On the contrary, the CVD-2 sample that comprises mainly small Au particles (d_i = 2–4 nm) demonstrates rather high catalytic activity under these conditions. In the presence of 43 mg of this catalyst containing 0.7 wt.% of Au, initial conversion of CO was 15% at GHSV = 60,000 h^{-1}, increased up to 35% during first 3 h and then remained unchanged till the end of the catalytic run. The apparent activation energy (E_a) for CO oxidation over the CVD-2 sample is only 9.5 kJ/mol (within the range of temperature from 40 to 90 °C), as calculated from the experimental Arrhenius plot of the steady-state catalyst activity shown in Fig. 14. This is close to the value of E_a = 7 kJ/mol reported by Goodman et al. [35,39] for CO oxidation at temperatures from 80 to 180 °C over the model catalysts

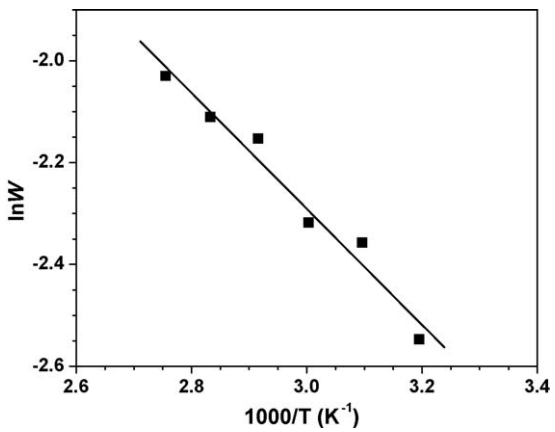

Fig. 14. Arrhenius plot of stationary rate (W, mol CO_2 (g Au c)$^{-1}$) of CO oxidation over the 0.7% Au/γ-Al_2O_{3ms} catalyst (Table 1, CVD-2 sample). *Reaction conditions:* A flow reactor; catalyst weight, 40 mg; atmospheric pressure; feed stream composition: 1% CO, 2.4% H_2O and 20% O_2 in N_2; GHSV, 60,000 h^{-1}.

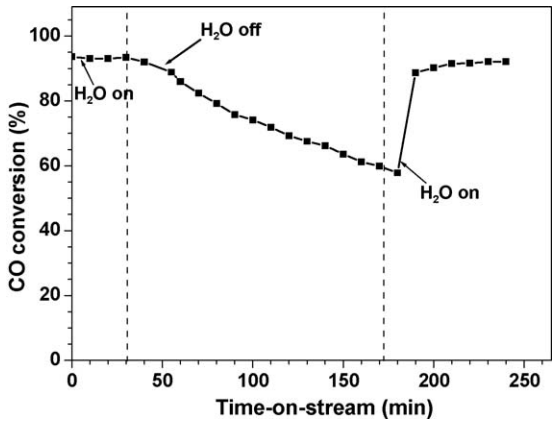

Fig. 15. Effect of H_2O on CO conversion during the CO + O_2 reaction over the 1.5% Au/δ-Al_2O_3 catalyst (Table 1, DP-2 sample). *Reaction conditions:* A flow reactor; temperature, 40 °C; atmospheric pressure; catalyst weight, 40 mg; feed stream composition: 1% CO, 2.4% H_2O and 20% O_2 in N_2; GHSV, 60,000 h^{-1}.

prepared by deposition of Au particles below 3.5 nm in diameter and 1 nm in height (2–3 atomic layers) on the TiO_2(1 1 0)-(1 × 1) surface. At the same time, our observed E_a value is much lower than the apparent activation energies for CO oxidation over various Pt and Pd catalysts which are typically ranged from 80 to 170 kJ/mol [9].

The catalytic performance of the Au/Al_2O_3 catalysts prepared by different methods (DP, impregnation, CVD) in CO oxidation is highly sensitive to the presence of moisture in the reaction feed, as illustrated in Fig. 15 with the 1.5% Au/δ-Al_2O_3 catalyst (Table 1, DP-2 sample) as an example. In the beginning of the catalytic run, while the feed was saturated with H_2O vapor (2.4 vol.%), the catalyst demonstrated a stable high activity in CO oxidation. As water vapor stopped being fed, the catalyst activity decreased with time-on-stream rapidly, but recovered completely in 10–15 min after water vapor feeding was resumed. This result is in good agreement with the literature data [40–42] that indicate a favorable influence of the presence of moisture in the reaction feed of CO oxidation on the catalytic performance of Au nanoparticles deposited on the oxide supports. This is another feature distinguishing Au catalysts from the conventional catalysts for CO oxidation, such as supported platinum group metals or bulk oxides of 3*d* and 4*d* metals (hopcalite, *etc.*), which are gradually deactivated by moisture. The data obtained are consistent with the mechanism of CO oxidation on supported Au catalysts proposed by Bond and Thompson [7,37] and, independently, by Kung et al. [38]. They assume that the active site for oxidation of CO represents an ensemble of metallic gold atoms including a minor amount of Au^+ (or Au^{3+}) cations coordinated with the OH groups. The metallic gold atoms serve as the sites for CO and O_2 adsorption. The CO + O_2 reaction is proposed to proceed *via* insertion of adsorbed CO molecules into Au^{x+}–OH complexes to form carboxylate species. Then the latter are oxidized to CO_2 by the adsorbed oxygen species. The presence of moisture in the reaction mixture is necessary for maintaining a sufficient concentration of Au^{x+}–OH species in the working catalyst. Even though this reaction mechanism was not conclusively proved, an important argument for its validity was reported by Gates and Guzman [43,44]. Using X-ray absorption near-edge spectroscopy (XANES) and a combination of temperature-programmed reduction (TPR) and temperature-programmed oxidation (TPO), they have found that both zero-valent Au and cationic Au are presented in the Au/MgO catalyst working under conditions of CO oxidation, the catalytic activity being dependent on the relative contents of Au^0 and Au^+.

3.3.2. Catalytic performance of Au catalysts for oxidation of CO contained in household air and simulated diesel exhaust

In this section, we shall demonstrate the results of testing of the nanodispersed Au/Al_2O_3 catalysts in CO oxidation under conditions which simulate in part some practical situations.

Table 3 presents the results obtained with the 1.4% Au/AOA-2 catalyst (Table 1, DP-5 sample) under standard conditions accepted in Russia for fast testing of the catalysts which are applied in the household air cleaning from carbon monoxide, that means room temperature, initial CO content of 450 ppm and relative air humidity 85% (for rest conditions see Section 2). A sample of the commercial 2.7% Pd/AOA-2 catalyst, which is widely used in air-cleaning devices of Russian production [45], was tested simultaneously. During the whole period of testing, the CO content in air stream passed through the Au/AOA-2 catalyst bed at GHSV of 20,000 h^{-1} remained on the level of 1–2 ppm that is lower by almost an order of magnitude than the CO concentration at the outlet of the reactor containing the Pd/AOA-2 catalyst, even though the precious metal content of the commercial catalyst is around twice that of the gold catalyst.

Another potential application of the gold catalysts is automobile pollution control. The catalytic efficiency of the highly dispersed Au/Al_2O_3 catalysts prepared in BIC has been tested for CO removal from the gas stream containing 0.1 vol.% CO, 10 vol.% H_2O, 14 vol.% O_2 and N_2 as a balance gas, whose composition simulated the characteristic features of diesel exhaust such as a comparatively high CO content in combination with higher steam content and some deficit of dioxygen as compared to their contents in air. Each catalyst sample was subjected to two to three successive runs of the determination of CO conversion (calculated from the difference over the inlet and outlet CO concentrations) as a function of temperature under programming temperature ramp from 30 to 300 °C. The commercial diesel oxidation catalyst containing platinum (2.3 wt.%) supported on δ-alumina and a β-zeolite as hydrocarbon trapping component (Al_2O_3/zeolite = 1.3/1, w/w) was tested under the same conditions for the sake of comparison.

Fig. 16 compares the temperature dependencies of CO conversion measured at a high space velocity of 200,000 h^{-1} with the commercial Pt–alumina–zeolite catalyst and the 1.4% Au/δ-Al_2O_3 catalyst prepared by the DP method and containing gold nanoparticles ($\langle d_l \rangle$ = 3.6 ± 1.3 nm, ($\langle d_{vs} \rangle$ = 4.4 nm). For the commercial Pt catalyst, the light-off curves are S-shaped that is typical of the CO oxidation over platinum metals and accounted for by the reaction that proceeds *via* the Langmuir–Hinshelwood mechanism [9]. At temperatures close to ambient, when the platinum surface is covered by adsorbed CO molecules which block the sites for O_2 adsorption, the CO conversion is low but rapidly increases with temperature to reach 50% at 88–92 °C and 100% at 110–120 °C (Fig. 16A). Meanwhile, the catalyst containing metallic Au nanoparticles with $\langle d_{vs} \rangle$ = 4.4 nm (as

Table 3
Comparison between the 1.4% Au/AOA-2 and commercial 2.7% Pd/AOA-2 catalysts for cleaning a wet air stream from CO under ambient conditions.

Duration of test (h)	Outlet CO concentration (ppm)		CO conversion (%)	
	Au catalyst	Pd catalyst	Au catalyst	Pd catalyst
1	<1	27	100	94.0
2	1	22	99.7	94.9
3	1	15	99.7	96.6
4	1.5	17	99.6	96.3
5	2	15	99.5	96.6
6	2	15	99.5	96.6
7	2	17	99.5	96.3

Reaction conditions: A flow reactor; temperature, 22–24 °C; atmospheric pressure; catalyst bed volume, 9.4 cm^3; feed stream composition, 450 ppm CO in air (air humidity 85%); GHSV, 20,000 h^{-1}.

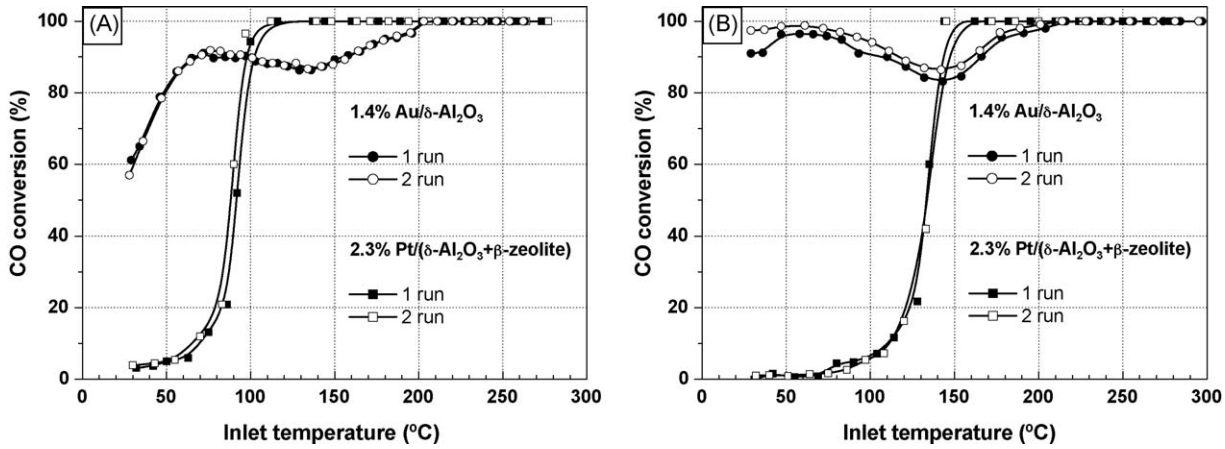

Fig. 16. Effect of reaction temperature on conversion of CO during the CO + O_2 reaction over the 2.3% Pt/(δ-Al_2O_3 + β-zeolite) (A) and 1.4% Au/δ-Al_2O_3 (B) catalysts tested (●, ○) in the as-prepared state and (■, □) after treatment at 700 °C for 4 h with an airflow containing 10 vol.% steam (thermal-steam aging). The curves marked by filled and open symbols correspond to the first and second temperature ramps, respectively. *Reaction conditions:* A flow reactor; atmospheric pressure; catalyst bed volume, 1.0 cm^3; feed stream composition: 0.1% CO, 10% H_2O and 14% O_2 in N_2; GHSV, 200,000 h^{-1}; heating rate, 10 °C/min.

measured by TEM) is much more active than the platinum catalyst at T = 30–80 °C. With the 1.4% Au/δ-Al_2O_3 catalyst, we failed to measure the light-off curves in their complete shape because the CO conversion was more than 50% at the temperature as low as 30 °C. This fact can be explained by much weaker Au–CO bonding in comparison to the Pt–CO bonding. As a result, CO molecules are desorbed from the metallic Au surface at lower temperatures than from the Pt surface. As we increase the reaction temperature from 70 to 150 °C, the CO conversion over the Au catalyst does not change or even slightly decreases (by 3–4%). Upon further temperature increasing, the CO conversion slowly increases to attain 100% at the temperature as high as 205 °C.

The data illustrated in Fig. 16 also allow us to compare the thermal and moisture stability of Au and Pt catalysts. As can be seen, calcination of the commercial Pt–alumina–zeolite catalyst in an airflow with a high steam content (10 wt.% H_2O) at 700 °C causes an increase in the temperatures for 50 and 100% conversion of CO (up to 134–135 °C and 145 °C, respectively). This thermal deactivation behavior is typical of platinum diesel oxidation catalysts [46]. On the contrary, after thermal-steam aging (Fig. 16B), the low-temperature activity of the 1.4% Au/δ-Al_2O_3 catalyst in CO oxidation increases (the CO conversion at 50 °C rises from 80 to 96–98%), at that the light-off curves exhibit an unusual shape showing the significant drop in CO conversion (down to 84% conversion) at moderate temperatures (70–145 °C). At higher temperatures the CO conversion over the thermally aged Au catalyst increases again, with temperature of 210–215 °C for 100% conversion. Hence, the results of the comparison demonstrate that in the low-temperature region (20–80 °C) the nanodispersed Au/Al_2O_3 catalyst provides a much higher degree of CO removal from the gas stream of the given composition than the commercial platinum–alumina–zeolite catalyst, the superiority of the gold catalyst becoming even more pronounced after thermal-steam aging of both catalysts. Our studies for the reasons of unusual properties of the gold–alumina catalysts for CO oxidation, such as their activation by treatment with air–steam mixture at a high temperature, the significant drop in CO conversion observed during the reaction temperature rise from *ca.* 70 to *ca.* 150 °C are in progress; the first results will be published in the nearest future.

4. Conclusion

1. The nanodispersed "gold on alumina" catalysts containing Au particles of 3–5 nm in diameter can be prepared with γ- and δ-Al_2O_3 as the supports using DP, IMP and CVD methods. The Au/Al_2O_3 catalysts prepared *via* adsorption of anionic Au hydroxide complexes from an alkalized $HAuCl_4$ solution (DP method) have the smallest in size metal particles and the narrowest size distribution. Impregnation of a support with an aqueous $HAuCl_4$ solution followed by reduction with H_2 is also a promising method to prepare small Au particles on Al_2O_3 with rather uniform size distribution provided that the amount of metal deposited is no more than 1.5–2 wt.%. The catalysts prepared by CVD are similar in Au particle sizes and size distribution to what we obtain by DP, if an organogold precursor is deposited on highly dehydrated alumina in a rotating reactor under *quasi-static* (not *flow*) conditions. Unlike the DP or IMP catalysts, the Au/Al_2O_3 catalysts prepared by CVD are characterized by the pronounced "egg shell" type distribution of the supported component. The "chemical liquid-phase grafting" method that means the physical adsorption of an organogold complex from a non-polar solvent gives the Au/Al_2O_3 samples containing only large metal crystallites with the mean diameter of around 15 nm in the absence of Au particles less than 5 nm in size.
2. Regardless of deposition technique (DP, IMP or CVD), the small Au particles ($d_i \leq 5$ nm) deposited onto γ- and δ-Al_2O_3, which are free of Cl^- impurity, are highly active toward catalytic combustion of CO in wet air stream under near-ambient conditions. Generally, the Au/Al_2O_3 catalysts prepared by DP demonstrate the highest activity in CO oxidation as compared with the CVD or impregnated catalysts, probably, due to the smaller mean Au particle diameter and narrower size distribution.
3. Diffuse reflectance UV–vis spectroscopy data in combination with the results of theoretical modeling of the spectra indicate that the active Au/Al_2O_3 catalysts prepared by DP method and calcined in air contain surface "ionic" Au species with bridging oxygen in addition to metallic Au nanoparticles. It would be well to take this fact into account when elucidating the detailed mechanism of low-temperature CO oxidation over Au/Al_2O_3 catalysts.
4. The results of testing of the nanodispersed Au/AOA-2 catalyst under conditions which simulate the polluted-air treatment show that the Au catalyst is more efficient for removal of CO in ambient air stream at room temperature than the commercial Pd/AOA-2 catalyst. Similarly, the Au/δ-Al_2O_3 catalyst prepared by DP in the low-temperature region ($T < 100$ °C) provides a much higher degree of CO removal from the gas stream whose composition simulates some characteristic features of diesel

engine exhaust, as compared with the commercial Pt–alumina–zeolite catalyst. At the same time, the Au catalyst is noticeably inferior to the Pt catalyst in the activity at high reaction temperatures apparently due to the lower activation energy for CO oxidation over Au nanoparticles. Therefore, it seems reasonable to use a gold catalyst in the exhaust treatment systems in combination with the platinum diesel oxidation catalyst, as it has been suggested in our patents [47].

5. Water vapor aids in promoting the catalytic activity of Au particles for CO oxidation. When the same catalyst, initially tested fresh, is then aged in an airflow containing of up to 10% steam at 700 °C and tested again, it is even more active compared to a sample that has not been subjected to the thermal-steam aging. A plausible origin of the effect is that the high concentration of the surface Au–OH and/or Al–OH groups participating in the catalytic cycle is needed for the maximal rate of CO oxidation.

Acknowledgements

The authors are grateful to their colleagues from the G.K. Boreskov Institute of Catalysis, Siberian Branch of the Russian Academy of Sciences (SB RAS), especially to Profs. V.F. Anufrienko, A.S. Ivanova and E.M. Moroz, Drs. T.V. Larina, S.Ph. Ruzankin, E.I. Vovk and D.A. Zyuzin, Mr. A.S. Bobrin, Mrs. I.L. Kraevskaya and Mr. E.P. Tikhomirov, as well as to Prof. P.P. Semyannikov, Dr. G.I. Zharkova and Mr. S.V. Trubin (from the A.V. Nikolaev Institute of Inorganic Chemistry, SB RAS), Dr. K.C.C. Kharas ('Range Fuels', USA) and Prof. B.E. Nieuwenhuys (University of Leiden, the Netherlands) for fruitful discussion and experimental contribution.

The authors thank financial support from the Integral Interdisciplinary Program of SB RAS (project no. 79). Also, this work was partially supported by the Dutch-Russian Research Cooperation Program which was conducted by the Netherlands Organization for Scientific Research and the Russian Foundation for Basic Research (grant No. 03-03-89012-NWO). One of the authors (P.A. P.) acknowledges the K. Zamaraev International Charitable Scientific Foundation for the financial support.

References

[1] M. Haruta, T. Kobayashi, H. Sano, N. Yamada, Chem. Lett. (1987) 405.
[2] M. Haruta, M. Date, Appl. Catal. A 222 (2001) 427.
[3] B. Grzybowska-Swierkosz, Catal. Today 112 (2006) 3.
[4] P. Claus, Appl Catal. A 291 (2005) 222.
[5] Q. Fu, H. Saltsburg, M. Flytzani-Stephanopoulos, Science 301 (2003) 935.
[6] D.T. Thompson, Nanotoday 2 (2007) 40, and references therein.
[7] G.C. Bond, D.T. Thompson, Gold Bull. 33 (2000) 41.
[8] M. Haruta, CATTECH 6 (2002) 102.
[9] M. Haruta, S. Tsubota, in: A. Wieckowski, E.R. Savinova, C.G. Constantinos (Eds.), Catalysis and Electrocatalysis at Nanoparticle Surface, Marcel Dekker, New York, 2003, p. 645.
[10] S. Tsubota, M. Haruta, T. Kobayashi, A. Ueda, Y. Nakahara, Stud. Surf. Sci. Catal. 63 (1991) 695.
[11] M. Okumura, M. Haruta, Chem. Lett. 4 (2000) 396.
[12] G.I. Zharkova, I.K. Igumenov, S.V. Zemskov, Koordinats. Khim. 6 (1980) 720 (in Russian).
[13] P.P. Semyannikov, B.L. Moroz, S.V. Trubin, G.I. Zharkova, P.A. Pyryaev, M.Yu. Smirnov, V.I. Bukhtiyarov, J. Struct. Chem. 47 (2006) 458.
[14] D. Briggs, M.P. Seach, Practical Surface Analysis, vol. 1, Wiley, Chichester (U.K.), 1992.
[15] J.A. Peck, C.D. Tarr, B.I. Swanson, G.E. Brown, Geohim. Cosmochim. Acta 55 (1991) 671.
[16] E.A. Nechaev, N.V. Nikolenko, Geokhimiya 33 (1985) 1656 (in Russian).
[17] A.B.P. Lever, Inorganic Electronic Spectroscopy, second ed., Elsevier, Amsterdam, 1984.
[18] A.L. Chuvilin, B.L. Moroz, V.A. Likholobov, J. Mol. Catal. 87 (1994) 231.
[19] V.F. Anufrienko, B.L. Moroz, T.V. Larina, V.I. Bukhtiyarov, V.N. Parmon, Dokl. Phys. Chem. 413 (2007) 75.
[20] B.L. Moroz, P.A. Pyryaev, V.I. Zaikovskii, S.Ph. Ruzankin, T.V. Larina, V.F. Anufrienko, V.I. Bukhtiyarov, in: V.N. Parmon, V.I. Bukhtiyarov, Z.R. Ismagilov (Eds.), Proceeding from the III International Conference "Catalysis: Fundamentals and Application", Part I, Boreskov Institute of Catalysis, Novosibirsk, 2007, p. 140.
[21] C.F. Bohren, D.R. Huffman, Adsorption and Scattering of Light by Small Particles, Wiley, New York, 1983.
[22] S.A. Yashnik, Z.R. Ismagilov, V.F. Anufrienko, Catal. Today 110 (2005) 310.
[23] C.G. Granqvist, R.A. Buhrman, J. Catal. 42 (1976) 477.
[24] D.Y. Cha, G. Parravano, J. Catal. 18 (1970) 200.
[25] M. Haruta, N. Yamada, T. Kobayashi, S. Iijima, J. Catal. 115 (1989) 301.
[26] G.R. Bamwenda, S. Tsubota, T. Nakamura, M. Haruta, Catal. Lett. 44 (1997) 83.
[27] R.J.H. Grisel, P.J. Kooyman, B.E. Nieuwenhuys, J. Catal. 191 (2000) 430.
[28] B.L. Moroz, P.A. Pyrjaev, V.I. Bukhtiyarov, in preparation.
[29] B. Hvolbaek, T.V.W. Janssens, B.S. Clausen, H. Falsig, C.H. Christensen, J.K. Norskov, Nanotoday 2 (2007) 14 (and references therein).
[30] J. Radnik, C. Mohr, P. Claus, Phys. Chem. Chem. Phys. 5 (2002) 172.
[31] M. Haruta, S. Tsubota, T. Kobayashi, H. Kageyama, M.J. Genet, B. Delmon, J. Catal. 144 (1993) 175.
[32] M. Herskowitz, R. Holliday, M.B. Cutlip, C.N. Kenney, J. Catal. 74 (1982) 408.
[33] E.I. Altman, R.J. Gorte, Surf. Sci. 172 (1986) 71.
[34] H.-S. Oh, C.C. Eickel, J. Catal. 128 (1991) 526.
[35] M.S. Chen, D.W. Goodman, Catal. Today 111 (2006) 22.
[36] C.K. Costello, J.H. Yang, H.Y. Lawa, Y. Wang, J.-N. Lin, L.D. Marks, M.C. Kung, H.H. Kung, Appl. Catal. A 243 (2003) 159.
[37] G.C. Bond, C. Louis, D.T. Thompson, Catalysis by Gold, IC Press, London, 2006.
[38] M.C. Kung, R.J. Davis, H.H. Kung, J. Phys. Chem. C 111 (2007) 11767.
[39] M. Valden, S. Pak, X. Lai, D.W. Goodman, Catal. Lett. 56 (1998) 7.
[40] H.-S. Oh, J.H. Yang, C.K. Costello, Y.M. Wang, S.R. Bare, H.H. Kung, M.C. Kung, J. Catal. 210 (2002) 375.
[41] C.K. Costello, M.C. Kung, H.-S. Oh, Y. Wang, H.H. Kung, Appl. Catal. 232 (2002) 159.
[42] M. Date, M. Haruta, J. Catal. 201 (2001) 221.
[43] J. Guzman, B.C. Gates, J. Phys. Chem. B 106 (2002) 7659.
[44] J. Guzman, B.C. Gates, J. Am. Chem. Soc. 126 (2004) 2672.
[45] T.L. Rakitskya, A.A. Ennan, V.Ya. Paina, Catalysts for Low-Temperature Oxidation of Carbon Monoxide, Khimneftemash, Moscow, 1991 (in Russian).
[46] J. Andersson, M. Antonsson, L. Eurenius, E. Olsson, M. Skoglundth, Appl. Catal. B 72 (2007) 71.
[47] B.L. Moroz, K.C.C. Kharas, M.Y. Smirnov, A.S. Bobrin, V.I. Bukhtiyarov, US Patent 019-7244A1 (2005); Eur. Patent 1570895 (2007).